Instant tough bioadhesive with triggerable benign detachment

Xiaoyu Chen[a,1], Hyunwoo Yuk[a,1], Jingjing Wu[a], Christoph S. Nabzdyk[b], and Xuanhe Zhao[a,c,2]

[a]Department of Mechanical Engineering, Massachusetts Institute of Technology, Cambridge, MA 02139; [b]Department of Anesthesiology and Perioperative Medicine, Mayo Clinic, Rochester, MN 55905; and [c]Department of Civil and Environmental Engineering, Massachusetts Institute of Technology, Cambridge, MA 02139

Edited by John A. Rogers, Northwestern University, Evanston, IL, and approved May 26, 2020 (received for review April 4, 2020)

Bioadhesives such as tissue adhesives, hemostatic agents, and tissue sealants have potential advantages over sutures and staples for wound closure, hemostasis, and integration of implantable devices onto wet tissues. However, existing bioadhesives display several limitations including slow adhesion formation, weak bonding, low biocompatibility, poor mechanical match with tissues, and/or lack of triggerable benign detachment. Here, we report a bioadhesive that can form instant tough adhesion on various wet dynamic tissues and can be benignly detached from the adhered tissues on demand with a biocompatible triggering solution. The adhesion of the bioadhesive relies on the removal of interfacial water from the tissue surface, followed by physical and covalent cross-linking with the tissue surface. The triggerable detachment of the bioadhesive results from the cleavage of bioadhesive's cross-links with the tissue surface by the triggering solution. After it is adhered to wet tissues, the bioadhesive becomes a tough hydrogel with mechanical compliance and stretchability comparable with those of soft tissues. We validate in vivo biocompatibility of the bioadhesive and the triggering solution in a rat model and demonstrate potential applications of the bioadhesive with triggerable benign detachment in ex vivo porcine models.

bioadhesive | wet adhesion | dry cross-linking | triggerable | hydrogel

Each year, multiple millions of major surgeries are performed worldwide (1). Whereas sutures and staples are most commonly used in these surgeries to close wounds, achieve hemostasis, and attach implantable devices on tissues, bioadhesives including tissue adhesives, hemostatic agents, and tissue sealants have been intensively studied as an alternative to sutures and staples because of their potential advantages such as ease of use, airtight or watertight sealing, and minimal tissue damage (2–8). However, most commercially available bioadhesives suffer from limitations including slow adhesion formation, weak bonding, low biocompatibility, poor mechanical match with tissues, and/or lack of triggerable benign detachment (3–5, 8, 9). To address these challenges, several bioadhesives have been developed in recent years including mussel-inspired adhesives (10, 11), nanoparticle solutions (12), tough hydrogel adhesives (13, 14), ultraviolet (UV)-curable tissue adhesive glues (15, 16), and tissue double-sided tapes (17). Despite these recent developments, to the best of our knowledge, there exists no bioadhesive that can both form fast tough adhesion with wet tissues and be benignly detached from the adhered tissues on demand. In particular, the triggerable benign detachment of bioadhesives is critical to repositioning misplaced bioadhesives and to retrieving implanted devices (4, 9). Whereas a few reversible adhesives have been developed (18–22), they commonly rely on harsh triggering conditions such as concentrated metallic ions, heat, or UV irradiation for the detachment, which are not favorable for bioadhesives and the adjacent native tissues.

Here, we report a bioadhesive that can form instant (within 5 s) and tough (interfacial toughness over 400 J m^{-2}) adhesion on various wet dynamic tissues and can be benignly detached from the adhered tissues on demand. The bioadhesive consists of interpenetrating networks of polyvinyl alcohol (PVA) and poly(acrylic acid) (PAA) grafted with cleavable *N*-hydroxysuccinimide (NHS) ester in the dry state. The instant adhesion of the bioadhesive relies on the removal of interfacial water from the wet tissue surface by the highly hygroscopic PAA network in the bioadhesive (Fig. 1*A*), which simultaneously forms instant physical cross-linking such as hydrogen bonds and electrostatic interactions to the tissue surface (17). Subsequent covalent cross-linking of the cleavable NHS ester in the bioadhesive with primary amine groups on the tissue surface further improves the long-term adhesion stability and strength (Fig. 1*A*). The triggerable detachment of the bioadhesive relies on the cleavage of the bioadhesive's physical and covalent cross-links with the tissue surface by a biocompatible triggering solution consisting of sodium bicarbonate (SBC) and glutathione (GSH) (Fig. 2 *B* and *C*). After it is adhered to wet tissues, the bioadhesive becomes a tough hydrogel with the low shear modulus (20 kPa) and high stretchability (seven times) comparable with those of soft tissues. We validate the in vivo biocompatibility of the bioadhesive and the triggering solution based on dorsal subcutaneous implantation in a rat model. We further provide ex vivo demonstrations of the potential applications of the bioadhesive with triggerable benign detachment including repositioning of a misplaced bioadhesive to seal an air leak in a porcine lung and on-demand retrieval of a bioadhesive device from a beating porcine heart.

Significance

Owing to potential advantages including ease of use, airtight or watertight sealing, and minimal tissue damage, bioadhesives have been intensively studied and developed as an alternative to sutures and staples to close wounds, achieve hemostasis, and attach and immobilize implantable devices. However, existing bioadhesives have limitations including slow adhesion formation, weak bonding, low biocompatibility, poor mechanical match with tissues, and/or lack of triggerable benign detachment. In this work, we report a bioadhesive capable of instant tough adhesion and triggerable benign detachment that can potentially address all the above-mentioned limitations. The current work not only develops a bioadhesive with superior performances but also advances the understanding of wet adhesion.

Author contributions: H.Y., C.S.N., and X.Z. designed research; X.C., H.Y., and J.W. performed research; X.C. and H.Y. contributed new reagents/analytic tools; X.C., H.Y., and X.Z. analyzed data; and X.C., H.Y., and X.Z. wrote the paper.

Competing interest statement: X.C., H.Y., and X.Z. are inventors on a patent application (US No. 63/034,644) that covers the instant tough bioadhesive with triggerable benign detachment.

This article is a PNAS Direct Submission.

[1]X.C. and H.Y. contributed equally to this work.

[2]To whom correspondence may be addressed. Email: zhaox@mit.edu.

This article contains supporting information online at https://www.pnas.org/lookup/suppl/doi:10.1073/pnas.2006389117/-/DCSupplemental.

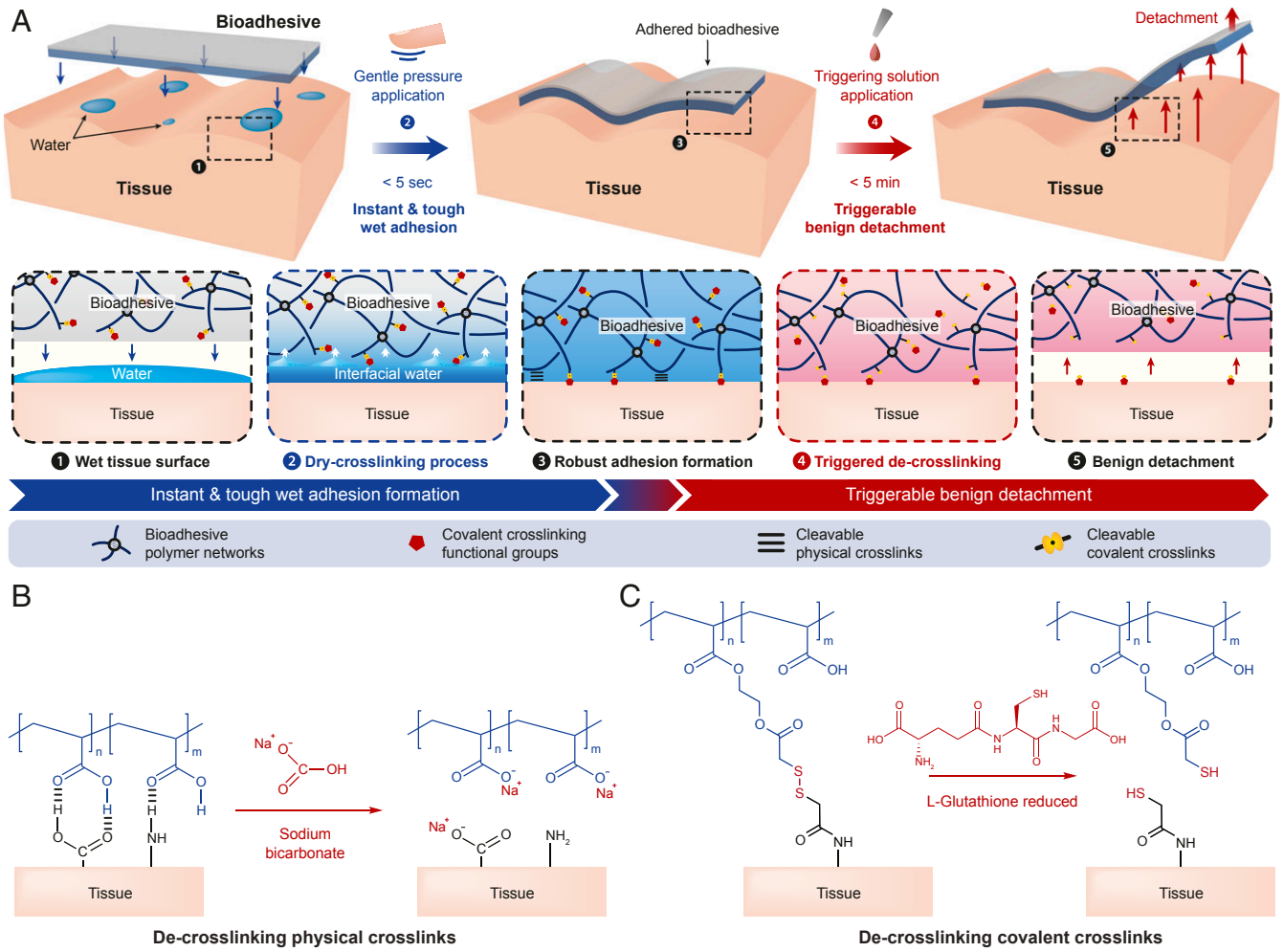

Fig. 1. Design and mechanisms of the instant, tough, and triggerably detachable bioadhesive. (*A*) Schematic illustration of design of the bioadhesive and dry cross-linking and triggerable detachment mechanisms. (*B*) Schematic illustrations for the de-cross-linking process of cleavable physical cross-links by SBC. (*C*) Schematic illustrations for the de-cross-linking process of cleavable covalent cross-links by GSH.

Results and Discussion

Mechanism for Instant Tough Adhesion of Bioadhesive. In wet physiological environments, biological tissues are commonly covered with a thin layer of water (23, 24). Upon the application of bioadhesives, it becomes interfacial water between the tissue and the applied bioadhesive, and the presence of this interfacial water can substantially impede the formation of rapid and robust adhesion between the tissues and the bioadhesives (17). To achieve instant tough adhesion on wet tissues, our proposed bioadhesive adopts a dry cross-linking mechanism to remove the interfacial water and form adhesion on wet tissues (17, 25) (Fig. 1*A*). The hygroscopic PVA and PAA networks of the dry bioadhesive can absorb the interfacial water to dry the wet tissue surfaces under gentle pressure (e.g., 1 kPa) applied for less than 5 s (17, 25) (Fig. 1*A*). Simultaneously, the PAA network of the bioadhesive provides abundant carboxylic acid groups that can form instant physical cross-links (i.e., hydrogen bonds) with the tissue surface (17, 26) (Fig. 1*A* and *SI Appendix*, Fig. S1). Furthermore, the cleavable NHS ester groups grafted to the PAA network form stable covalent cross-links (i.e., amide bonds) with primary amine groups abundant on the tissue surface within a few minutes (27, 28) (Fig. 1*A* and *SI Appendix*, Fig. S1). After adhering to tissues, the swollen bioadhesive becomes a thin layer of highly stretchable tough hydrogel with stretchability over seven times and fracture toughness over 1,000 J m^{-2}, whose favorable mechanical properties are crucial to achieving tough adhesion of the bioadhesive (29–32).

Mechanism for Triggerable Detachment of Bioadhesive. Tough adhesion of the bioadhesive to the wet tissue surface relies on both physical and covalent cross-links whose relative contributions are varying at different timescales of adhesion. In the short term (<5 min), the instant physical cross-links (i.e., hydrogen bonds) dominate the adhesion between the bioadhesive and the tissue surface. The contribution of the physical cross-links to the adhesion decreases over time, as the equilibration and subsequent neutralization of carboxylic acid groups in the bioadhesive deprive the bioadhesive's ability to form physical cross-links with the tissue surface (Fig. 1*B* and *SI Appendix*, Fig. S1). Therefore, the contribution of the covalent cross-links (i.e., amide bonds) to the adhesion gradually increases in the longer term (*SI Appendix*, Fig. S1). The need for triggerable detachment of the bioadhesive may present broadly at different timescales, including immediately after application to reposition misplaced bioadhesives, within minutes to hours for intraoperative removal of temporary bioadhesives for definitive surgical repair, and after days to weeks in the case of a removal of implanted devices. Therefore, the bioadhesive should

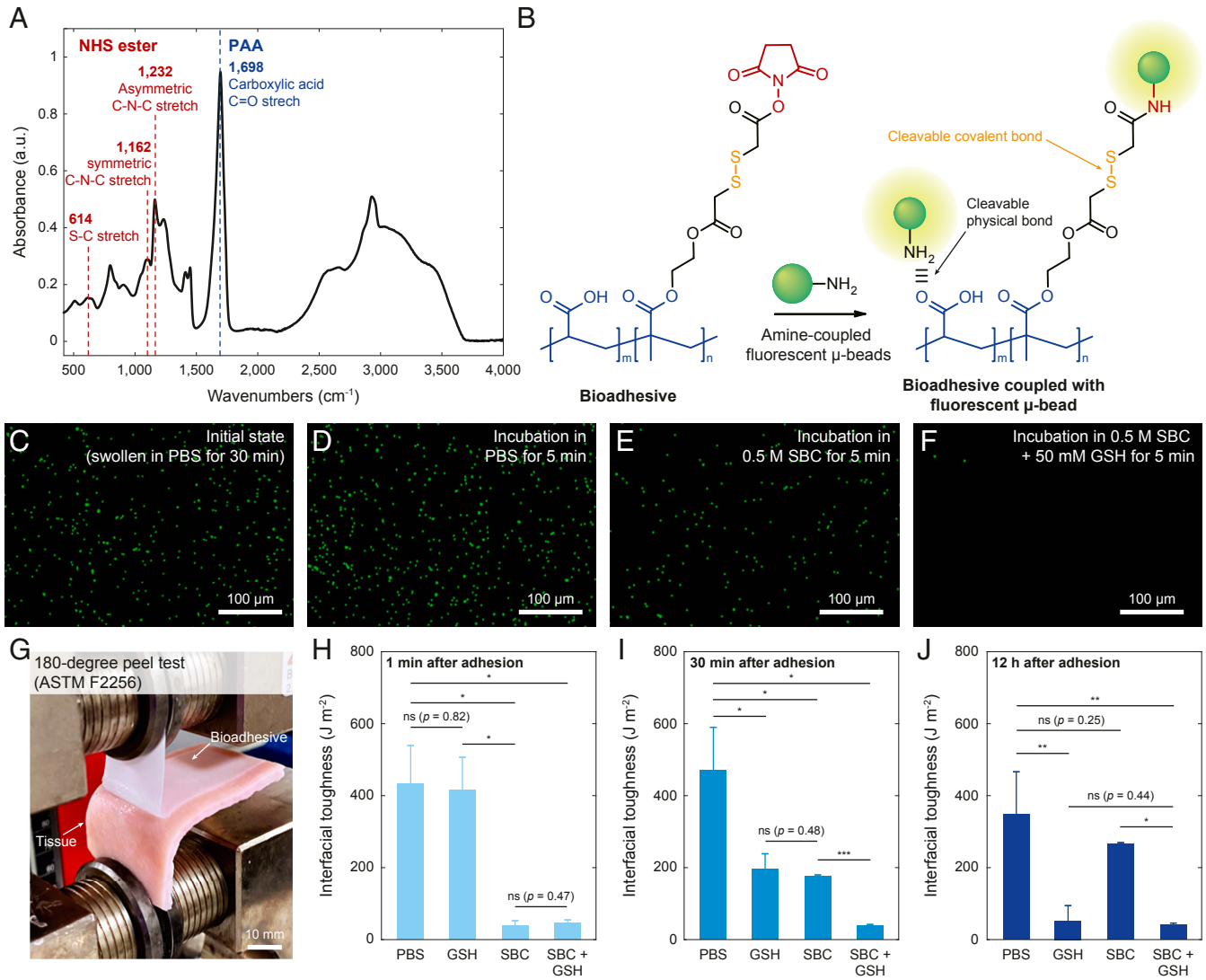

Fig. 2. Triggerable detachment of the bioadhesive. (*A*) FTIR spectra of the bioadhesive with associated peaks for carboxylic acid (1,698 cm^{-1}), disulfide (614 cm^{-1}), and NHS ester (1,162 and 1,232 cm^{-1}) functional groups. a.u., arbitrary unit. (*B*) Schematic illustrations for validation of triggerable detachment based on fluorescent primary amine-coupled microbeads. (*C–F*) Fluorescent microscope images for the bioadhesive sample in the initial state (*C*), 5 min after incubation in PBS (*D*), PBS with 0.5 SBC (*E*), and PBS with 0.5 M SBC and 50 mM GSH (*F*). (*G*) Photograph of 180° peel test setup for the measurement of interfacial toughness. (*H–J*) Interfacial toughness between the bioadhesive and wet porcine skin tissues 5 min after applying various solutions in short-term (*H*), intermediate-term (*I*), and long-term (*J*) adhesion. Values in *H–J* represent the mean and the SD ($n = 4$). *P* values are determined by a Student's *t* test. Scale bars are shown in the images. ns, not significant ($P > 0.05$). $*P \leq 0.05$; $**P \leq 0.01$.

be able to offer triggerable detachments in an effective and biocompatible manner across a broad time frame.

We design both physical and covalent cross-links of the bioadhesive to be on-demand cleavable by a biocompatible triggering solution (Fig. 1*A*). To cleave the physical cross-links, we adopt pH-dependent de-cross-linking of the physical cross-links of hydrogen bonds by SBC (33, 34) (Fig. 1*B*). To cleave the covalent cross-links, we introduce cleavable disulfide bonds between the NHS ester groups and the PAA network by synthesizing a functional monomer (*SI Appendix*, Figs. S2 and S3 show the synthesis of functional monomer and confirmation by ^{1}H NMR). Upon introduction of a biocompatible reducing agent such as GSH (35), a pendant thiol group in the GSH can break the disulfide bonds in the bioadhesive into thiol groups under physiological conditions (21, 36), cleaving the covalent cross-links between the bioadhesive and the tissue surface (Fig. 1*C*).

Evaluation of Performances of Adhesion and Triggerable Detachment. We first validate the successful incorporation of carboxylic acid (1,698 cm^{-1}), NHS ester (1,162 and 1,232 cm^{-1}), and disulfide (614 cm^{-1}) groups in the bioadhesive by the attenuated total reflection (ATR) Fourier transform infrared spectroscopy (FTIR) analysis (37) (Fig. 2*A*).

To validate the triggerable cleavage of the physical and covalent cross-links of the bioadhesive by the triggering solution (0.5 M SBC and 50 mM GSH in phosphate buffered saline [PBS]), we use primary amine-coupled fluorescent microbeads as a model to evaluate the adhesion and detachment between the bioadhesive and the amine-rich surfaces of the microbeads (Fig. 2*B*). A fluorescent microscope image of the bioadhesive incubated in PBS with the amine-coupled fluorescent microbeads for 30 min shows stably adhered microbeads on the bioadhesive, owing to the physical and covalent cross-links between the bioadhesive and the microbeads' surfaces (Fig. 2*C* and *SI Appendix*,

Fig. S4). We further incubate the bioadhesive with the fluorescent microparticles in PBS alone, PBS with 0.5 M SBC, and PBS with 0.5 M SBC and 50 mM GSH for 5 min. The bioadhesive incubated in PBS alone exhibits no significant change in the number of adhered fluorescent microbeads (Fig. 2*D* and *SI Appendix*, Fig. S4). The bioadhesive incubated in PBS with 0.5 M SBC shows a significant reduction in the number of adhered fluorescent microbeads, although a substantial portion of the microbeads remains adhered (Fig. 2*E* and *SI Appendix*, Fig. S4). In contrast, the bioadhesive incubated in PBS with 0.5 M SBC and 50 mM GSH exhibits nearly complete detachment of the adhered fluorescent microbeads (Fig. 2*F* and *SI Appendix*, Fig. S4). These results indicate that the adhesion of the microbeads' amine-rich surfaces on the bioadhesive is stable under physiological conditions and that their complete triggered detachment requires the cleavage of both physical cross-links (by SBC) and covalent cross-links (by GSH).

To investigate the effect of the proposed triggerable detachment mechanism on the adhesion performance, we measure the interfacial toughness between the bioadhesive and wet porcine skin tissues, following the standard test for tissue adhesives (180° peel test, ASTM F2256) (Fig. 2*G* and *SI Appendix*, Fig. S5). As shown in Fig. 2 *H–J*, the bioadhesive can form tough adhesion with interfacial toughness over 400 J m^{-2} on wet porcine skin tissues upon contact and gentle pressure (1 kPa) application for less than 5 s, demonstrating the capability of instant tough adhesion. Furthermore, the bioadhesive can form instant tough adhesion under various physiological pH conditions, potentially allowing its use in various places in the human body (*SI Appendix*, Fig. S6).

We next apply PBS alone, PBS with 50 mM GSH, PBS with 0.5 M SBC, and PBS with 0.5 M SBC and 50 mM GSH to the bioadhesive adhered to the porcine skin followed by the interfacial toughness measurements (*SI Appendix*, Figs. S7 and S8). For the short-term adhesion (triggering solutions applied 1 min after adhesion formation), the samples treated with the solutions containing SBC (PBS with 0.5 M SBC, PBS with 0.5 M SBC and 50 mM GSH) show a significant reduction in the measured interfacial toughness, while the samples treated with the solution containing GSH alone (PBS with 50 mM GSH) exhibit negligible difference to the samples treated with PBS alone (Fig. 2*H*). This means that SBC and its capability to cleave the physical cross-links play a critical role in the triggerable detachment of the short-term adhesion. For the intermediate-term adhesion (solutions applied 30 min after adhesion formation), all other samples exhibit a substantial decrease in the measured interfacial toughness compared with the samples treated with PBS alone. Also, the samples treated with the solution containing both SBC and GSH (PBS with 0.5 M SBC and 50 mM GSH) demonstrate significantly lower interfacial toughness than the samples treated with the solution containing either SBC or GSH (PBS with 50 mM GSH or PBS with 0.5 M SBC) (Fig. 2*I*). This means that both SBC and GSH and their capability to cleave the physical cross-links and the covalent cross-links play a critical role in the triggerable detachment of the bioadhesive after intermediate-term adhesion. For the long-term adhesion (solutions applied 12 h after adhesion formation), the samples treated with the solutions containing GSH (PBS with 50 mM GSH and PBS with 0.5 M SBC and 50 mM GSH) show significant lower interfacial toughness than other samples. Also, the samples treated with the solution containing SBC alone (PBS with 0.5 M SBC) exhibit negligible difference from the samples treated with PBS alone (Fig. 2*J*). This means that GSH and its capability to cleave the covalent cross-links play a critical role in triggerable detachment of the long-term adhesion. These results validate that the triggering solution of PBS with 0.5 M SBC and 50 mM GSH can cleave both physical cross-links (by SBC) and covalent cross-links (by GSH) and substantially decrease the interfacial toughness across a broad time frame after the formation of adhesion (Fig. 1 and *SI Appendix*, Fig. S1).

Evaluation of In Vivo Applicability and Biocompatibility. To evaluate the bioadhesive's capability of forming rapid, robust, and triggerably detachable adhesion to wet tissues in vivo, we adhere the bioadhesive to a muscular layer of a rat subcutaneous space followed by a triggered detachment of the bioadhesive on demand (Fig. 3*A*). We find that the bioadhesive can be adhered to the muscular layer of the rat after gently pressing for 5 s, forming adhesion robust enough to resist pulling apart by tweezers. To detach the adhered bioadhesive on demand, we apply the triggering solution in the subcutaneous space of the rat for 5 min, which allows benign removal of the bioadhesive patch without observable damage to the underlying tissue surface (Fig. 3*A*). We further evaluate the in vivo biocompatibility of the bioadhesive and the triggerable detachment process in a rat dorsal model of subcutaneous implantation (Fig. 3 *B–E*). The histological assessment made by a blinded pathologist indicates that the triggering solution and the triggerable detachment process generate a mild inflammatory reaction comparable with that generated by the sham control group (surgery without implantation) at 2 wk after the surgeries (Fig. 3 *B*, *C*, and *E*). Furthermore, the histological assessment of the bioadhesive implanted for 2 wk shows a mild to moderate inflammatory reaction (Fig. 3 *D* and *E*). These results support the biocompatibility of the bioadhesive and the triggerable detachment of the bioadhesive.

Potential Applications. Triggerable and atraumatic on-demand detachment of bioadhesives can find potential applications in various clinical scenarios in different time frames. In the short term, the bioadhesives can accidentally be applied incorrectly on the tissue surface, which requires the immediate correction for appropriate surgical treatment. In such clinical scenarios, the triggerable detachment of the bioadhesive can allow prompt revision of the incorrectly applied bioadhesive without causing damage to the underlying tissue (38). In the intermediate term, emergency treatments of clinically unstable patients frequently require subsequent definitive surgical repair after the initial surgery. In such clinical scenarios, the triggerable detachment of the bioadhesive can allow on-demand removal of the bioadhesive during the definitive surgical repair after temporary organ sealing for the initial damage control surgeries over hours. In the long term, various medical devices such as cannulae and drains in cardiac surgeries and drug depots in localized cancer chemotherapies require subsequent removal after several days to weeks of implantation. In such clinical scenarios, the instant tough bioadhesive with triggerable detachment can provide both secure fixations as well as atraumatic retrieval of the devices.

To investigate potential applications of the benignly detachable bioadhesive, we demonstrate ex vivo proof of principle applications on porcine organs. To demonstrate potential advantages of the instant tough adhesion and triggerable benign detachment of our bioadhesive in such situations, we show the successful repositioning of a bioadhesive that initially only incompletely sealed a lacerated porcine lung (3-cm incision) (Fig. 4*A* and Movie S1). As shown in Fig. 4*B*, the incorrectly adhered bioadhesive can be easily removed in a facile and benign manner within 5 min after applying the triggering solution. Importantly, subsequent application of a new bioadhesive yields the rapid formation of airtight sealing of the porcine lung (Movie S1) without compromising the adhesion performance (*SI Appendix*, Fig. S9).

In another example, we demonstrate instant robust integration and on-demand removal of bioadhesive devices on wet dynamic tissues. Since many devices are not readily permeable to the triggering solution, we design a patterned bioadhesive to facilitate the transport and diffusion of the triggering solution to the adhesion interface (Fig. 4*C*). As shown in Fig. 4*D*, a patterned

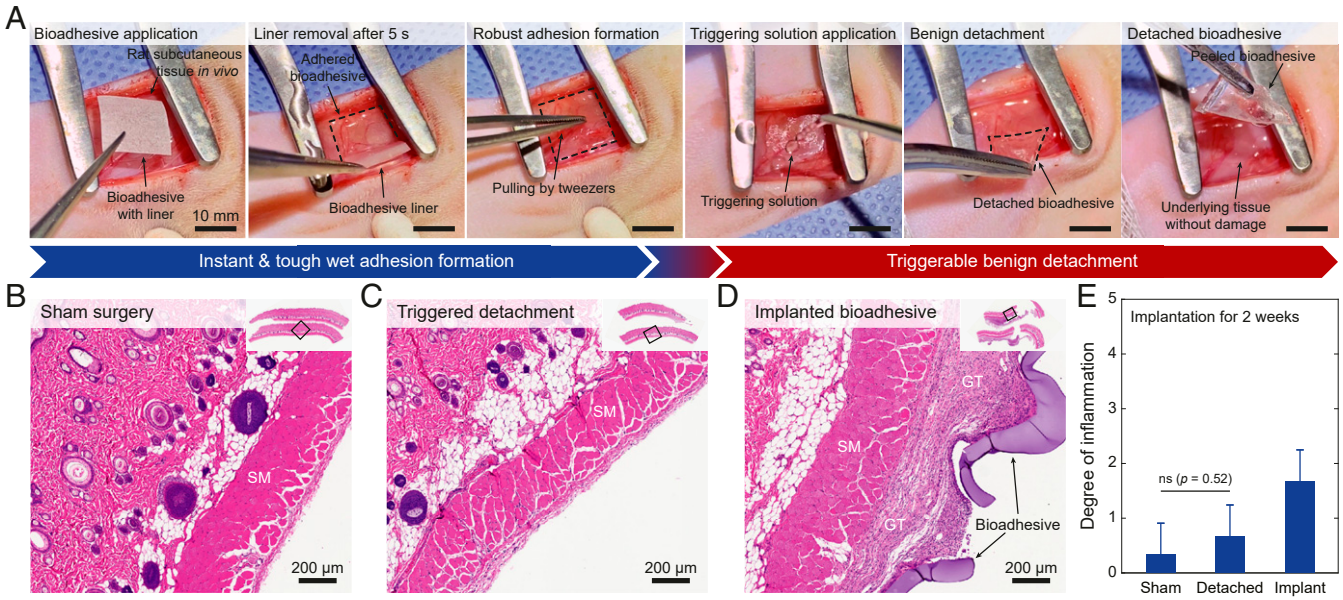

Fig. 3. In vivo applicability and biocompatibility of the bioadhesive. (*A*) Photographs for instant robust adhesion and triggerable benign detachment of the bioadhesive in rat subcutaneous space in vivo. (*B–D*) Representative histological images stained with H&E for biocompatibility assessment of the sham surgery (*B*), the triggered detachment of the bioadhesive (*C*), and the implanted bioadhesive (*D*). (*E*) Degree of inflammation of the sham surgery, the triggered detachment of the bioadhesive, and the implanted bioadhesive groups evaluated by a blinded pathologist (0, normal; 1, very mild; 2, mild; 3, moderate; 4, severe; 5, very severe) after 2 wk of subcutaneous implantation. SM and GT indicate skeletal muscle and granulation tissue, respectively. All experiments are repeated four times with similar results. Values in *E* represent the mean and the SD ($n = 4$). *P* values are determined by a Student's *t* test. Scale bars are shown in the images. ns, not significant ($P > 0.05$).

bioadhesive on an impermeable thermoplastic polyurethane film allows facile transport and diffusion of the triggering solution (red colored by a food dye) across the adhered device. We further demonstrate that a mock device consisting of a gold-coated polyimide and a patterned bioadhesive can form rapid and robust adhesion onto a beating ex vivo porcine heart (by introducing pressurized air inputs to mimic heartbeats) and can be removed on demand (Fig. 4*E* and Movie S2). Owing to the instant tough adhesion capability of the bioadhesive, the bioadhesive device can form robust and stable adhesion on the beating porcine heart within 5 s of application (Movie S2). Also, the application of the triggering solution allows benign and atraumatic removal of the adhered device in 5 min (Fig. 4*F*). The bioadhesive's capability to form instant robust adhesion on wet dynamic tissues and be benignly detached on demand may find particular advantages for integration and potential atraumatic removal of implantable devices.

Conclusion

In summary, we report a bioadhesive that synergistically incorporates the mechanisms of dry cross-linking and cleavable bonds to enable its instant tough adhesion on wet tissues and triggerable benign detachment from the adhered tissues, respectively. We systematically investigate the mechanisms, adhesion and triggerable detachment performances, and in vivo applicability and biocompatibility as well as proof of principle applications of the proposed bioadhesive to facilitate its clinical adoption and translation. The unique advantages of the instant tough bioadhesive with triggerable benign detachment can potentially address the limitations of existing tissue adhesives and may broaden the applications of bioadhesives in practice. This study not only offers a promising tissue adhesive with superior performances but also, advances the understanding of reversible wet adhesion for the development of future adhesives in wet environments.

Materials and Methods

Synthesis of NHS Ester Functionalized Monomer with Disulfide Bond. To prepare NHS ester functionalized monomer with disulfide bond, 2,2′ disulfanediyldiacetic acid (1.8 g, 10.0 mmol) and acetic anhydride (8.0 mL) were added to a 100-mL round-bottomed flask equipped with a magnetic stirring bar. The mixture was stirred at room temperature for 3 h to obtain a homogeneous solution (*SI Appendix*, Fig. S2*A*). Then, the solvent was removed in vacuo to afford 1,4,5-oxadithiepane-2,7-dione as a light-yellow oil. The oil was directly transferred into the mixture of 2-hydroxyethyl methacrylate (1.9 g, 15.0 mmol), 4-dimethylaminopyridine (12.0 mg, 1.0 mmol), and 15 mL anhydrous dichloromethane (DCM). The solution was stirred at room temperature overnight, and then, the reaction was finalized by adding 30 mL of saturated $NaHCO_3$ solution (*SI Appendix*, Fig. S2*B*). Then, the mixture was acidified with 1 M HCl to pH = 2.0 and extracted with DCM. The organic phase was dried over Na_2SO_4 and concentrated under reduced pressure. The crude product was purified by flash column chromatography on silica gel with a mixture of MeOH and DCM (vol/vol = 1/20) as the eluent to afford 6-(2-(methacryloyloxy)ethoxy)hept-6-enoic acid. The 6-(2-(methacryloyloxy) ethoxy)hept-6-enoic acid (2.94 g, 10.0 mmol) was then dissolved in 30 mL anhydrous DCM and stirred with NHS (1.15 g, 10 mmol) in an ice bath for 30 min. Then, 1-[3-(dimethylamino)propyl]-3-ethylcarbodiimide hydrochloride (1.55 g, 10 mmol) in 20 mL DCM was added dropwise into the above mixture. The solution was stirred overnight under a nitrogen atmosphere at room temperature (*SI Appendix*, Fig. S2*C*). The crude product was purified by flash column chromatography on silica gel with a mixture of petroleum ether and ethyl acetate (vol/vol = 1/1) as the eluent to afford the product as a colorless liquid. ^{1}H NMR (400 MHz, $CDCl_3$, δ): 6.17 (p, 1H, -CH2), 5.59 (q, 1H, -CH2), 4.44 to 4.33 (m, 4H, -OCH2CH2O-), 3.83 to 3.68 (d, 4H, -CH2SSCH2-), 2.85 (s, -CH2-CH2-), 1.94 (s, 3H, -CH3) (*SI Appendix*, Fig. S3).

Preparation of the Bioadhesive. To prepare the bioadhesive, PVA (Mw = 146,000 to 186,000, 7 wt/wt %), acrylic acid (35 wt/wt %), α-ketoglutaric acid (0.2 wt/wt %), and poly(ethylene glycol methacrylate) (Mn = 550, 0.05 wt/wt %) were dissolved in deionized water. Then, we dissolved 100 mg functional monomer (NHS ester functionalized monomer with disulfide bond) in 1 mL acetone and added to 10 mL of the above stock solution to get a precursor solution. The precursor solution was then poured on a glass mold with spacers (the thickness is 210 μm unless otherwise mentioned) and cured in a UV light chamber (284-nm, 10-W power) for 30 min. As a nonadhesive layer,

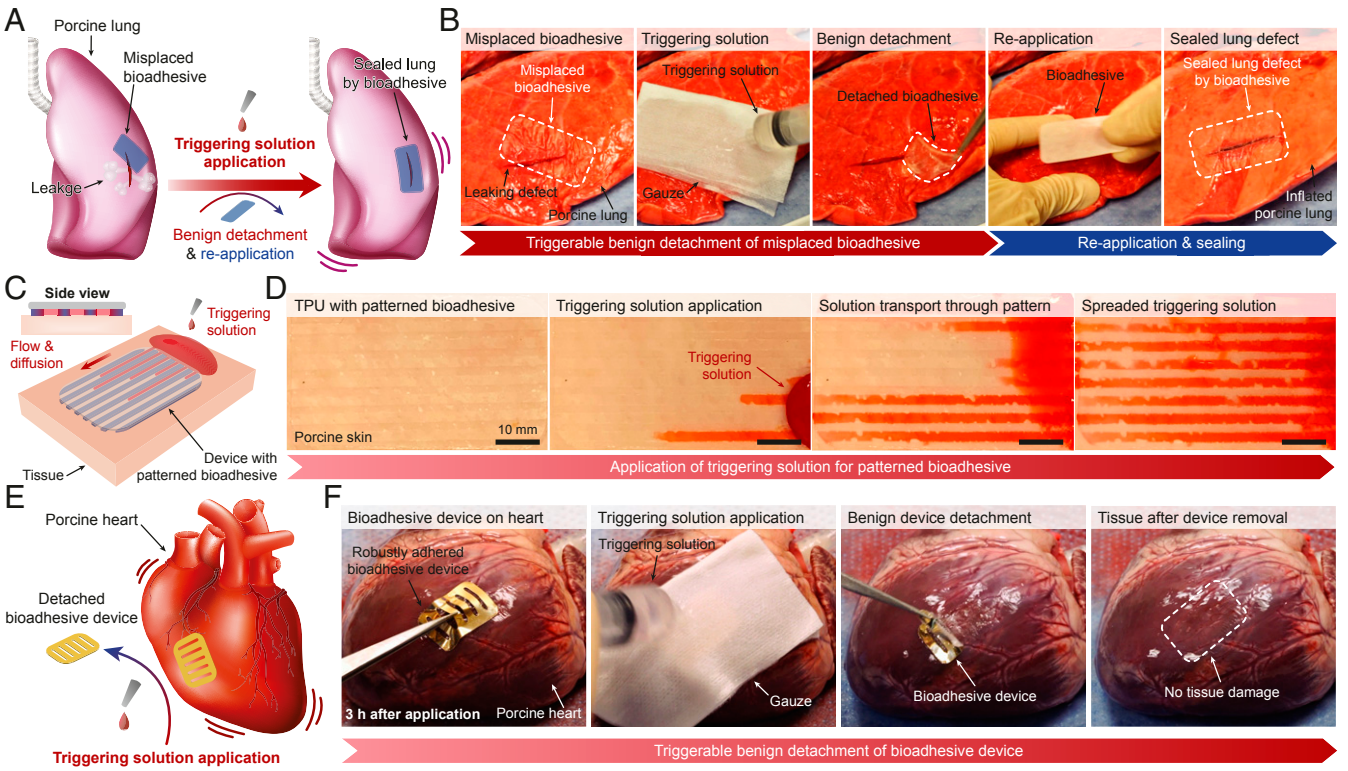

Fig. 4. Potential applications of the bioadhesive. (*A* and *B*) Schematic illustrations (*A*) and photographs (*B*) for correction of a misplaced bioadhesive and instant sealing of a lacerated ex vivo porcine lung by the bioadhesive. (*C* and *D*) Schematic illustrations (*C*) and photographs (*D*) for a patterned bioadhesive for facile transport and diffusion of the triggering solution for impermeable devices. (*E* and *F*) Schematic illustrations (*E*) and photographs (*F*) for instant robust adhesion and on-demand removal of a bioadhesive device on a beating ex vivo porcine heart. TPU, thermoplastic polyurethane.

10 wt/wt % thermoplastic polyurethane solution was spin coated on the cured bioadhesive at 400 rpm for 30 s and dried completely. The prepared bioadhesives were sealed in plastic bags with desiccant (silica gel packets) and stored at –20 °C before use. To pattern the bioadhesive, a large sheet of bioadhesive was cut into various patterns using a laser cutter (Epilog). Weighing paper (VWR) was used as a removable liner for the bioadhesive.

Preparation of the Triggering Solution. To prepare the triggering solution, 0.5 M SBC and L-glutathione reduced (GSH) were dissolved in PBS. The triggering solution was filtered by using a 0.2-μm sterile syringe filter before use. For validation of the triggerable detachment of the bioadhesive, the bioadhesive was incubated in PBS with primary amine-coupled fluorescent microbeads (FluoSpheres; Thermo Fisher Scientific) for 30 min in room temperature. Then, the samples were further incubated in various triggering solutions for 5 min followed by thorough washing with clean PBS to remove nonadhered microparticles. The presence of the adhered microbeads was characterized by using a fluorescence microscope (LV10; Nikon), and the number of the adhered microbeads was counted by using ImageJ.

Mechanical Tests. For tissue samples stored more than 10 min before mechanical tests, the samples were covered with a large amount of 0.01 wt/vol % sodium azide solution (in PBS) spray and sealed in plastic bags to prevent degradation and dehydration of the tissues. Unless otherwise indicated, all tissues and engineering solids were adhered to by the benignly detachable bioadhesive after washout of the surfaces with PBS followed by 5 s of pressing (with 1-kPa pressure applied by either mechanical testing machine or equivalent weight). To measure interfacial toughness, adhered samples with widths of 2.5 cm were prepared and tested by the standard 180° peel test (ASTM F2256) using a mechanical testing machine (2.5-kN load cell; Zwick/Roell Z2.5). All tests were conducted with a constant peeling speed of 50 mm min^{-1}. The measured force reached a plateau as the peeling process entered the steady state. Interfacial toughness was determined by dividing two times the plateau force by the width of the tissue sample (*SI Appendix*, Fig. S5). Hydrophilic nylon filters (1-μm pore size; TISCH Scientific) were applied as a stiff backing for the bioadhesive. Poly(methyl methacrylate) films (with a thickness of 50 μm; Goodfellow) were applied using cyanoacrylate glue (Krazy Glue) as a stiff backing for the tissues. Unless otherwise indicated, the interfacial toughness was measured 5 min after applying the triggering solution.

FTIR Characterization. Chemical composition of the bioadhesive was characterized by a transmission Fourier transform infrared spectroscope (FTIR 6700; Thermo Fisher) using a Germanium ATR crystal (55°).

In Vivo Biocompatibility Evaluation. All animal surgeries were reviewed and approved by the Committee on Animal Care at the Massachusetts Institute of Technology. Female Sprague–Dawley rats (225 to 250 g; Charles River Laboratories) were used for all in vivo studies. Before implantation, the bioadhesive was prepared using aseptic techniques and was further sterilized for 3 h under UV light. For implantation in the dorsal subcutaneous space, rats were anesthetized using isoflurane (1 to 2% isoflurane in oxygen) in an anesthetizing chamber. Anesthesia was maintained using a nose cone. The back hair was removed, and the animals were placed over a heating pad for the duration of the surgery. The subcutaneous space was accessed by a 1- to 2-cm skin incision per implant in the center of the animal's back. To create space for implant placement, blunt dissection was performed from the incision toward the animal shoulder blades. For the sham surgery group, no implant was placed in the subcutaneous pocket ($n = 4$). For the triggerable detachment group, the bioadhesive (10 × 20 mm) was placed in the subcutaneous pocket created above the incision and detached 5 min after applying 1 mL of the triggering solution ($n = 4$). For the bioadhesive implantation group, the bioadhesive (10 mm in width and 20 mm in length) was placed in the subcutaneous pocket created above the incision without detachment ($n = 4$). The incision was closed using interrupted sutures (4-0 Vicryl; Ethicon), and 3 to 6 mL of saline was injected subcutaneously. Up to three implants were placed per animal, ensuring no overlap between each subcutaneous pocket created. After 2 wk following the implantation, the animals were euthanized by CO_2 inhalation; subcutaneous regions of interest were excised and fixed in 10% formalin for 24 h for histological analyses.

Histological Processing. Fixed tissue samples were placed into 70% ethanol and submitted for histological processing and Hematoxylin and Eosin (H&E) staining at the Hope Babette Tang (1983) Histology Facility in the Koch Institute for Integrative Cancer Research at the Massachusetts Institute of Technology. Histological assessment was performed by a blinded pathologist on a scale of zero to five (zero, normal or absent; one, very mild or minimal; two, mild; three, moderate; four, severe or marked; five, very severe) to evaluate the degree of inflammation in the tissues surrounding the implants. The degree of acute inflammation was based on the number of neutrophils. The degree of chronic inflammation was based on the presence of lymphocytes, macrophages, and plasma cells. The degree of inflammation was evaluated based on the overall presence of indicators in each histological sample (absent, minimal, mild, moderate, or marked presence). Representative images of each group were shown in the corresponding figures.

Ex Vivo Tests. All ex vivo experiments were reviewed and approved by the Committee on Animal Care at the Massachusetts Institute of Technology. For the correction of misplaced bioadhesive, a laceration was made on a porcine lung lobe with a razor blade (3 cm in length). The air was then applied through the tubing connected to the upper part of the trachea (25-mmHg pressure) to visualize air leakage. A bioadhesive (2.5 cm in width and 5 cm in length) was applied on the damaged lung lobe with 5 s of pressing to partially cover the laceration to represent misplacement and incomplete sealing. The misplaced bioadhesive was covered with medical gauze, and the triggering solution was applied to the gauze. Five minutes after the application of the triggering solution, the misplaced bioadhesive was removed by tweezers. To seal the exposed laceration, a new bioadhesive was applied to fully cover the laceration, and the airtight sealing was confirmed by cyclic inflation and deflation of the porcine lung.

For the adhesion and on-demand removal of bioadhesive device, a mock device with gold-coated polyimide and patterned bioadhesive (2 cm in width and 4 cm in length, bioadhesive pattern with 1-mm width and 1.5-mm gap) was adhered on a beating ex vivo porcine heart. An aorta of the heart was connected to tubing, and programmed pressurized air inputs were introduced into the porcine heart by using a microdispenser (Ultimus V; Nordson EFD) to mimic heartbeats. The adhered device on the beating heart was kept for 3 h at room temperature and then checked for robust adhesion by pulling with tweezers. The bioadhesive device was covered with medical gauze, and the triggering solution was applied to the gauze. Five minutes after the application of the triggering solution, the bioadhesive device was removed by tweezers, and the surface of the porcine heart was examined for tissue damage. For experiments longer than 1 h in ambient condition, a wet towel soaked with 0.01 wt/vol % sodium azide solution (in PBS) was covered on the heart to prevent dehydration and degradation.

Statistical Analysis. MATLAB software was used to assess the statistical significance of all comparison studies in this work. Data distribution was assumed to be normal for all parametric tests but not formally tested. In the statistical analysis for comparison between multiple samples, one-way ANOVA followed by Tukey's multiple comparison test was conducted with the thresholds of $*P \leq 0.05$, $**P \leq 0.01$, and $***P \leq 0.001$. In the statistical analysis between two data groups, a two-sample Student's t test was used, and the significance thresholds were placed at $*P \leq 0.05$, $**P \leq 0.01$, and $***P \leq 0.001$.

Data Availability. All data are available in the text, *SI Appendix*, or Movies S1 and S2.

ACKNOWLEDGMENTS. We thank the Koch Institute Swanson Biotechnology Center for technical support, specifically K. Cormier and the Histology Core for the histological processing and Dr. R. Bronson at Harvard Medical School for the histological analyses. This work is supported by NSF Grant EFMA-1935291. H.Y. acknowledges financial support from Samsung Scholarship.

1. T. G. Weiser *et al*., An estimation of the global volume of surgery: A modelling strategy based on available data. *Lancet* **372**, 139–144 (2008).
2. A. J. Singer *et al*., Prospective, randomized, controlled trial of tissue adhesive (2-octylcyanoacrylate) vs standard wound closure techniques for laceration repair. Stony brook octylcyanoacrylate study group. *Acad. Emerg. Med.* **5**, 94–99 (1998).
3. P. Coulthard *et al*., Tissue adhesives for closure of surgical incisions. *Cochrane Database Syst. Rev.* **5**, CD004287 (2010).
4. T. B. Reece, T. S. Maxey, I. L. Kron, A prospectus on tissue adhesives. *Am. J. Surg.* **182** (suppl. 2), 40S–44S (2001).
5. H. Khoshmohabat, S. Paydar, H. M. Kazemi, B. Dalfardi, Overview of agents used for emergency hemostasis. *Trauma Mon.* **21**, e26023 (2016).
6. P. Hangge *et al*., Hemostasis and nanotechnology. *Cardiovasc. Diagn. Ther.* **7** (suppl. 3), S267–S275 (2017).
7. J. Yang, R. Bai, B. Chen, Z. Suo, Hydrogel adhesion: A supramolecular synergy of chemistry, topology, and mechanics. *Adv. Funct. Mater.* **30**, 1901693 (2020).
8. G. M. Taboada *et al*., Overcoming the translational barriers of tissue adhesives. *Nat. Rev. Mater.* **5**, 310–329 (2020).
9. N. Annabi, K. Yue, A. Tamayol, A. Khademhosseini, Elastic sealants for surgical applications. *Eur. J. Pharm. Biopharm.* **95**, 27–39 (2015).
10. B. P. Lee, P. B. Messersmith, J. N. Israelachvili, J. H. Waite, Mussel-inspired adhesives and coatings. *Annu. Rev. Mater. Res.* **41**, 99–132 (2011).
11. C. E. Brubaker, P. B. Messersmith, The present and future of biologically inspired adhesive interfaces and materials. *Langmuir* **28**, 2200–2205 (2012).
12. S. Rose *et al*., Nanoparticle solutions as adhesives for gels and biological tissues. *Nature* **505**, 382–385 (2014).
13. J. Li *et al*., Tough adhesives for diverse wet surfaces. *Science* **357**, 378–381 (2017).
14. J. Yang, R. Bai, Z. Suo, Topological adhesion of wet materials. *Adv. Mater.* **30**, e1800671 (2018).
15. N. Lang *et al*., A blood-resistant surgical glue for minimally invasive repair of vessels and heart defects. *Sci. Transl. Med.* **6**, 218ra6 (2014).
16. Y. Hong *et al*., A strongly adhesive hemostatic hydrogel for the repair of arterial and heart bleeds. *Nat. Commun.* **10**, 2060 (2019).
17. H. Yuk *et al*., Dry double-sided tape for adhesion of wet tissues and devices. *Nature* **575**, 169–174 (2019).
18. Y. Zhao *et al*., Bio-inspired reversible underwater adhesive. *Nat. Commun.* **8**, 2218 (2017).
19. Y. Zhou *et al*., Light-switchable polymer adhesive based on photoinduced reversible solid-to-liquid transitions. *ACS Macro Lett.* **8**, 968–972 (2019).
20. Y. Gao, K. Wu, Z. Suo, Photodetachable adhesion. *Adv. Mater.* **31**, e1806948 (2019).
21. W. Li *et al*., Tough bonding, on-demand debonding, and facile rebonding between hydrogels and diverse metal surfaces. *Adv. Mater.* **31**, e1904732 (2019).
22. T. Xie *et al*., Wound dressing change facilitated by spraying zinc ions. *Mater. Horiz.* **7**, 605–614 (2020).
23. R. Michel *et al*., Interfacial fluid transport is a key to hydrogel bioadhesion. *Proc. Natl. Acad. Sci. U.S.A.* **116**, 738–743 (2019).
24. K. Li, S. Cai, Wet adhesion between two soft layers. *Soft Matter* **10**, 8202–8209 (2014).
25. X. Mao, H. Yuk, X. Zhao, Hydration and swelling of dry polymers for wet adhesion. *J. Mech. Phys. Solids* **137**, 103863 (2020).
26. Y. Wang *et al*., Instant, tough, noncovalent adhesion. *ACS Appl. Mater. Interfaces* **11**, 40749–40757 (2019).
27. M. J. E. Fischer, "Amine coupling through EDC/NHS: A practical approach" in *Surface Plasmon Resonance (Methods and Protocols)*, N. Mol, M. J. E. Fischer, Eds. (Methods in Molecular Biology, Humana Press, New York, NY, 2010), Vol. 627, pp. 55–73.
28. C. Wang, Q. Yan, H.-B. Liu, X.-H. Zhou, S.-J. Xiao, Different EDC/NHS activation mechanisms between PAA and PMAA brushes and the following amidation reactions. *Langmuir* **27**, 12058–12068 (2011).
29. H. Yuk, T. Zhang, S. Lin, G. A. Parada, X. Zhao, Tough bonding of hydrogels to diverse non-porous surfaces. *Nat. Mater.* **15**, 190–196 (2016).
30. H. Yuk, T. Zhang, G. A. Parada, X. Liu, X. Zhao, Skin-inspired hydrogel-elastomer hybrids with robust interfaces and functional microstructures. *Nat. Commun.* **7**, 12028 (2016).
31. T. Zhang, H. Yuk, S. Lin, G. A. Parada, X. Zhao, Tough and tunable adhesion of hydrogels: Experiments and models. *Lixue Xuebao* **33**, 543–554 (2017).
32. C. Creton, J. Hooker, K. R. Shull, Bulk and interfacial contributions to the debonding mechanisms of soft adhesives: Extension to large strains. *Langmuir* **17**, 4948–4954 (2001).
33. T. Wang, E. Canetta, T. G. Weerakkody, J. L. Keddie, U. Rivas, pH dependence of the properties of waterborne pressure-sensitive adhesives containing acrylic acid. *ACS Appl. Mater. Interfaces* **1**, 631–639 (2009).
34. R. S. Gurney *et al*., Mechanical properties of a waterborne pressure-sensitive adhesive with a percolating poly(acrylic acid)-based diblock copolymer network: Effect of pH. *J. Colloid Interface Sci.* **448**, 8–16 (2015).
35. S. D. Perreault, R. A. Wolff, B. R. Zirkin, The role of disulfide bond reduction during mammalian sperm nuclear decondensation in vivo. *Dev. Biol.* **101**, 160–167 (1984).
36. J. Liu *et al*., Triggerable tough hydrogels for gastric resident dosage forms. *Nat. Commun.* **8**, 124 (2017).
37. K. Oberg, B. A. Chrunyk, R. Wetzel, A. L. Fink, Nativelike secondary structure in interleukin-1 beta inclusion bodies by attenuated total reflectance FTIR. *Biochemistry* **33**, 2628–2634 (1994).
38. A. Mattick, Use of tissue adhesives in the management of paediatric lacerations. *Emerg. Med. J.* **19**, 382–385 (2002).

PNAS
www.pnas.org

Supplementary Information for

Instant tough bioadhesive with triggerable benign detachment

Xiaoyu Chen[1†], Hyunwoo Yuk[1†], Jingjing Wu[1], Christoph S. Nabzdyk[2], Xuanhe Zhao[1,3*]

[1]Department of Mechanical Engineering, Massachusetts Institute of Technology, Cambridge, MA 02139, USA
[2]Department of Anesthesiology and Perioperative Medicine, Mayo Clinic, Rochester, MN 55905, USA
[3]Department of Civil and Environmental Engineering, Massachusetts Institute of Technology, Cambridge, MA 02139, USA

† Xiaoyu Chen and Hyunwoo Yuk contributed equally to this work.

* Corresponding author: Xuanhe Zhao
Email: zhaox@mit.edu

This PDF file includes:

Figures S1 to S9
Legends for Movies S1 to S2

Other supplementary materials for this manuscript include the following:

Movies S1 to S2

www.pnas.org/cgi/doi/10.1073/pnas.2006389117

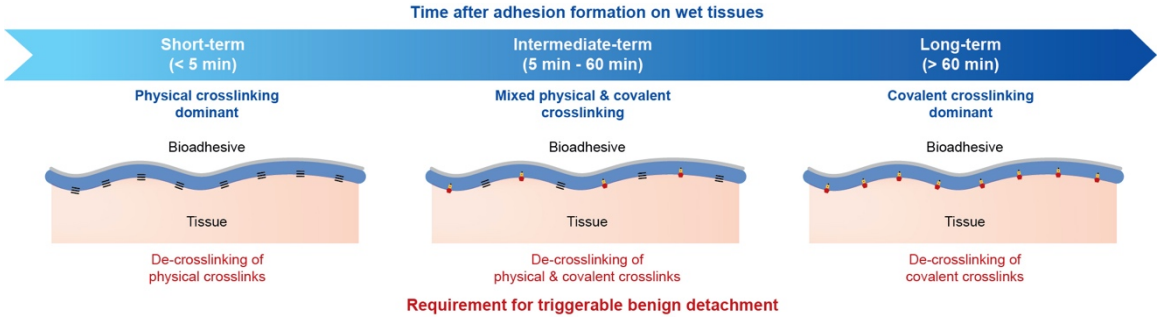

Fig. S1. Schematic illustrations for the different timescales of adhesion and the corresponding requirement for triggerable benign detachment of the bioadhesive.

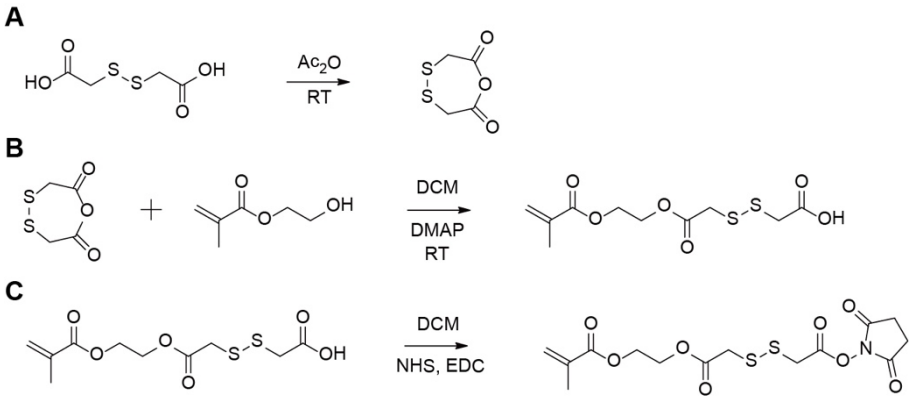

Fig. S2. Chemical schemes for the synthesis of functional monomer.

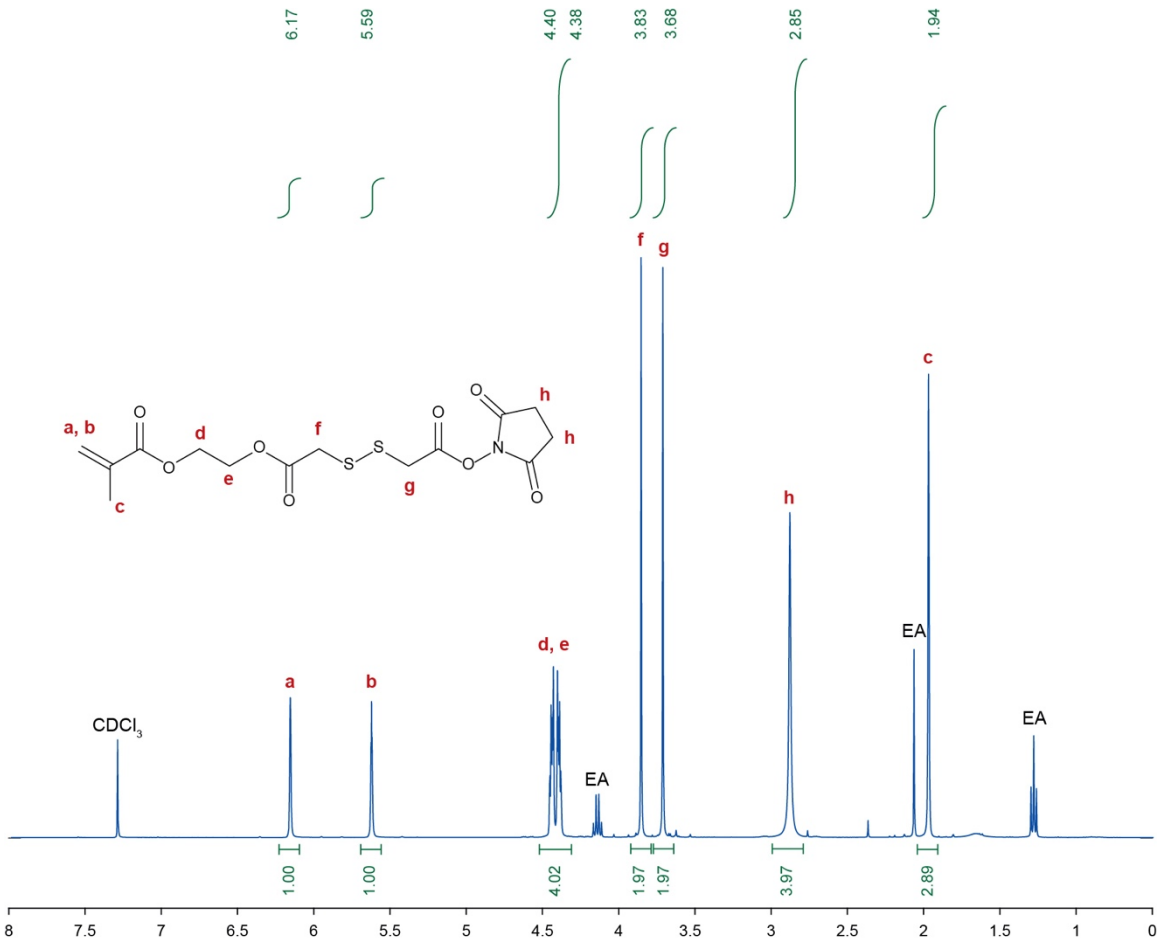

Fig. S3. ^{1}H NMR spectra for synthesized NHS ester functionalized monomer with a disulfide bond.

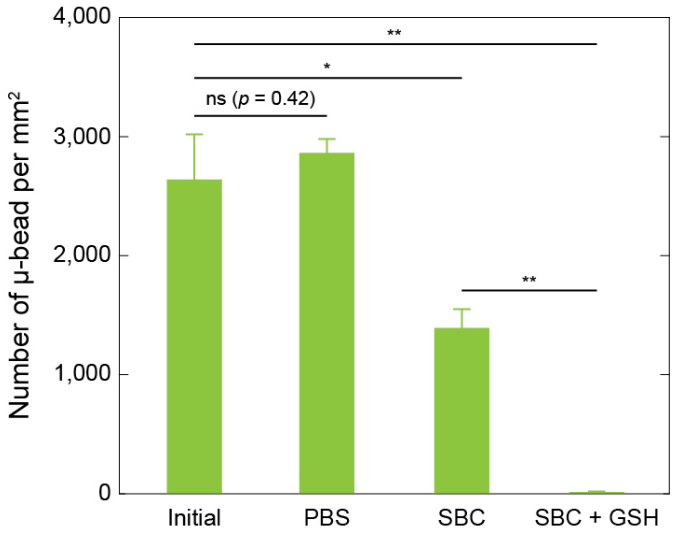

Fig. S4. The number of adhered fluorescent microbeads on the bioadhesive 5 min after incubation in varying solutions in Fig. 2*C-F*. Values represent the mean and the standard deviation (n = 4). *P* values are determined by a Student's *t*-test; ns, not significant ($p > 0.05$); * $p \leq 0.05$; ** $p \leq 0.01$.

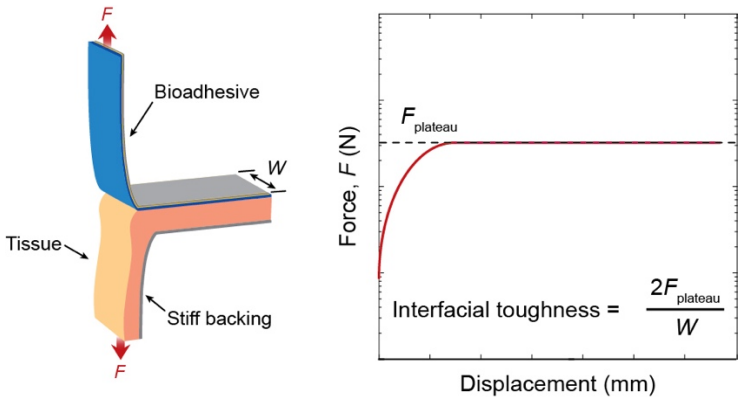

Fig. S5. Mechanical testing setups for interfacial toughness measurements based on the standard 180-degree peel test (ASTM F2256).

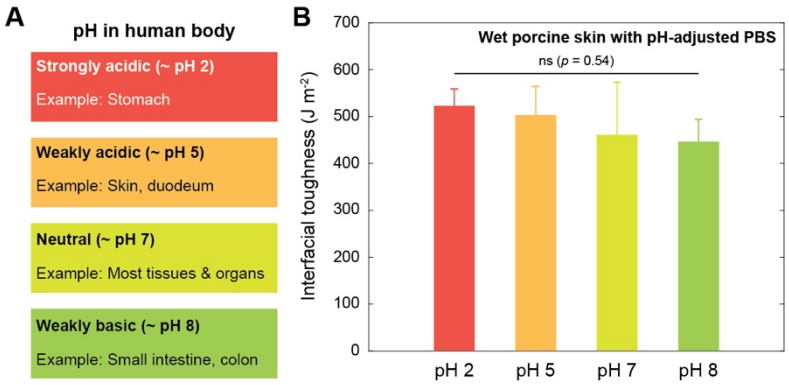

Fig. S6. Effect of pH on the adhesion performance. (*A*) Various pH values in human body. (*B*) Interfacial toughness between the bioadhesive and wet porcine skin tissues incubated in various pH-adjusted PBS. Values in (B) represent the mean and the standard deviation (n = 3). *P* values are determined by one-way ANOVA and Tukey's multiple comparison test; ns, not significant (p > 0.05).

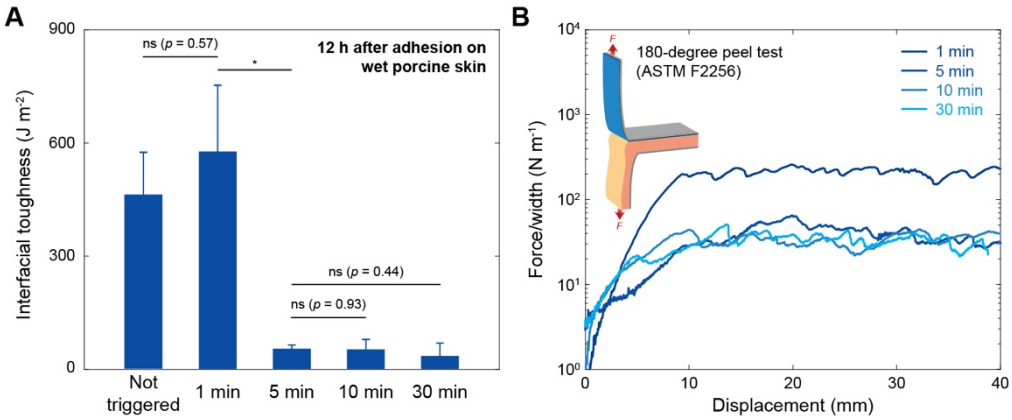

Fig. S7. The efficiency of the triggerable detachment of the bioadhesive. (*A*) Interfacial toughness between the bioadhesive and wet porcine skin tissues without triggering and 1, 5, 10, and 30 min after the application of the triggering solution. (*B*) Representative force/width vs. displacement curves for the 180-degree peel tests. Values in (A) represent the mean and the standard deviation (n = 4). *P* values are determined by a Student's *t*-test; ns, not significant ($p > 0.05$); * $p \leq 0.05$.

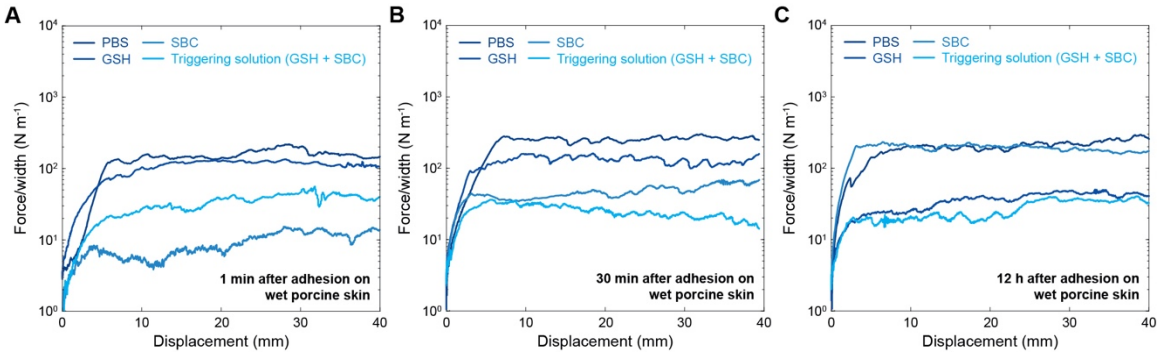

Fig. S8. (*A*-*C*) Representative force/width vs. displacement curves for the 180-degree peel tests of short-term (A), intermediate-term (B), and long-term (C) adhesion in Fig. 2*H*-*J*.

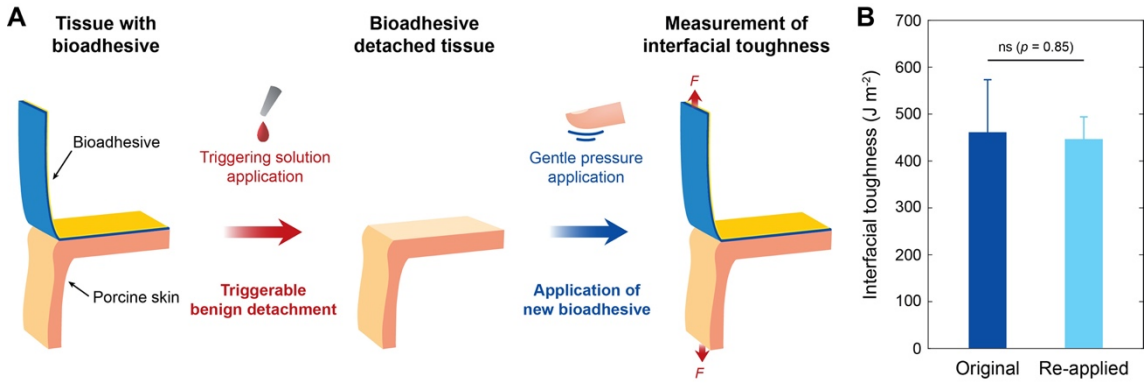

Fig. S9. Effect of triggerable detachment and re-application of bioadhesive on the adhesion performance. (*A*) Schematic illustrations for triggerable detachment and re-application of the bioadhesive. (*B*) Interfacial toughness between wet porcine skin tissues and the bioadhesive originally applied and re-applied on the same tissue after triggerable detachment. Values in (B) represent the mean and the standard deviation (n = 3). *P* values are determined by a Student's *t*-test; ns, not significant ($p > 0.05$).

Movie S1. Triggerable benign detachment and re-application of bioadhesive for sealing of *ex vivo* porcine lung.

Movie S2. Triggerable benign detachment of bioadhesive device from beating *ex vivo* porcine heart.